OBSERVATIONS AND ANALYSIS TO DEVELOP PERFORMANCE REQUIREMENTS FOR A LIVING SNOW FENCE DURING SEVERE SNOWSTORM EVENTS

Yusuke Harada[1]*, Akihiro Yoshii[1], Satoshi Omiya[1] and Atsushi Nishimura[1]

[1] *Civil Engineering Research Institute for Cold Region, Public Works Research Institute, Sapporo, Japan*

ABSTRACT: In this study, we conducted observations on trees, snowdrifts, and meteorological elements related blowing snow using a shelterbelt composed of evergreen conifers to investigate the design methodology of living snow fences in a severe snowstorm. Based on the results, we created the average distribution of leaf area density on the survey lines and organized the relationship between the shelterbelt and the meteorological data in a snowstorm.

KEYWORDS: Living Snow Fences, Severe snowstorm events, Performance requirements

1. INTRODUCTION

In recent years, the cold snowy regions of Japan have occasionally seen more incidents of vehicles being stuck in snow and road closures due to severe snowstorms caused by rapidly developed low-pressure systems and convergence zones. Living Snow Fences (hereinafter: "LSFs") have been installed along roadsides to mitigate blowing snow since 1976 in Hokkaido, northern part of Japan, which reduce road traffic problems such as snowdrifts and poor visibility (CERI, 2011). The extent of LSFs in Hokkaido totaled approximately 100 km as of 2020 (Sakurai et al., 2023). According to “The Highway Snowstorm Countermeasure Manual”, the standard width of an LSF along the national highways is classified into three types; 10 m, 20 m, and 30 m, where the maximum volume of snow settled at snowdrifts is 20 m^3 m^{-1} or greater referring to previous experiences in Japan (CERI, 2011). However, there is no established design methodology based on the performance requirements for LSFs considering severe snowstorm events in Japan. Therefore, we conducted observations on trees, snowdrifts, and meteorological elements related blowing snow to investigate the design methodology of LSFs.

2. OBSERVATION METHODS

2.1 Study site

The study site was the Ishikari blowing snow test field of the Civil Engineering Research Institute for Cold Region, which is located in southwest Hokkaido in the northern part of Japan (N43°12’, E141°23’). The prevailing wind direction during blowing snow in the field was WNW. We carried out observation on trees, snowdrifts, and meteorological elements related blowing snow to investigate the design methodology, using a linear shelterbelt of approximately 80 m long and 15-30 m wide consisting mainly of Pinaceae, located north to south in the field. Here, there set three survey lines (in the W-E direction) orthogonal to the shelterbelt (see Figure 1).

2.2 Tree observation

We conducted the tree observation to find out the structure and leaf area of the shelterbelt using a drone with LiDAR and a camera (DJI Matricce300RTK and ZemuseL1). We acquired point cloud data and images (approximately 80 m long and wide) on Dec. 2nd, 2022 (the early winter of 2022/23). The LiDAR measurements were performed under three angle conditions: vertical downward (0°), oblique (45°), and lateral (60°) using iterative and non-iterative scanning as shown in Figure 1. Using raw scan data, point cloud data (3D XYZ data) in LAS format was created by the software (DJI Terra). The LAS data including precipitation particles was manually cleaned up using point cloud editing software (CloudCompare). Using the camera images of a wrap rate of 80 %, an ortho-image (GeoTIFF) of the observation area was created by the method of Structure-from-Motion/Multi-View-Stereo (SfM-MVS).

At three survey lines before the winter as shown in Figure 1, ground-level surveys were firstly conducted using automatic level and total station. Next, tree surveys were conducted by the belt transect method (width = 10 m) to acquire tree height, diameter at breast height, the crown width, and the height of the crown base (see Figure 2, Figure 3, and Figure 4). In addition, the survey getting leaf area index (m^2 m^{-2}) (hereinafter: "LAI") was conducted by a plant canopy analyzer (LI-COR LAI-2000, hereinafter: "PCA"), and a fisheye camera (Nikon D600, and SIGMA 8mm F3.5 EX DG Circular Fisheye). Images taken by

* *Corresponding author address:*
Yusuke Harada, Civil Engineering Research Institute for Cold Region, PWRI, 1-3-1-34 Hiragishi, Toyohira-ku, Sapporo, Hokkaido 062-8602;
tel: +81-11-841-1746; fax: +81-11-841-9747;
email: harada-y@ceri.go.jp

the fisheye camera were analyzed using the software of LIA32 (Yamamoto, 2008), and Gap Light Analyzer (Simon Fraser University, 1999) (see Figure 2 and Figure 4).

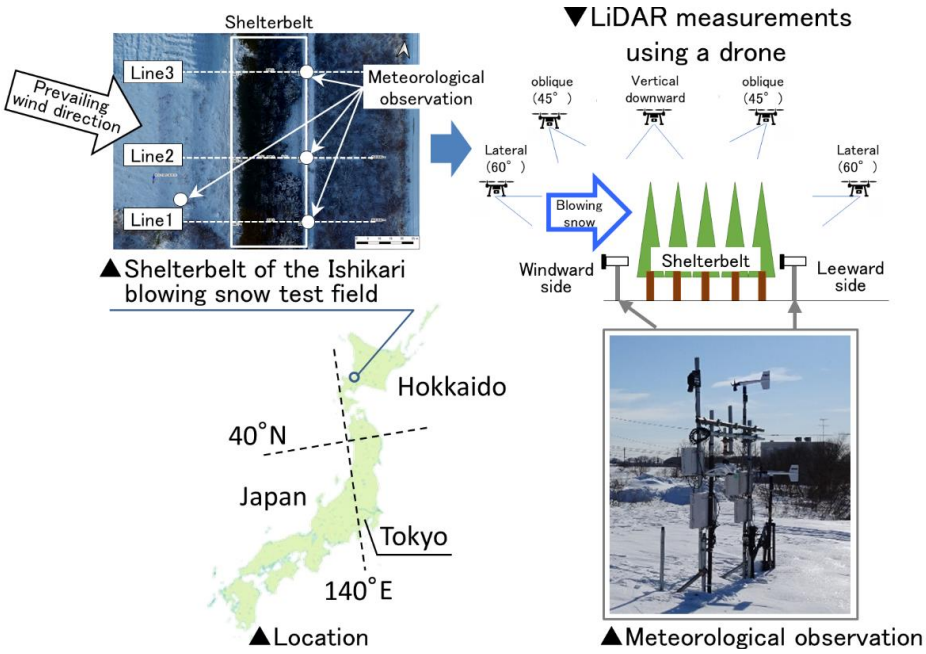

Figure 1: Description of the study site.

Figure 2: Tree observation in the shelterbelt: left, tree surveys; center, LAI using a PCA; right, LAI using a fisheye camera.

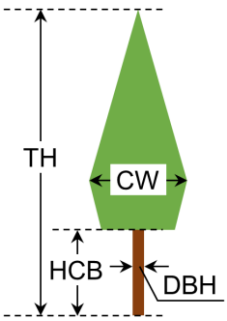

TH : tree heights
DBH : diameter at breast height
CW : crown width
HCB : height of crown base

Figure 3: Items of tree survey.

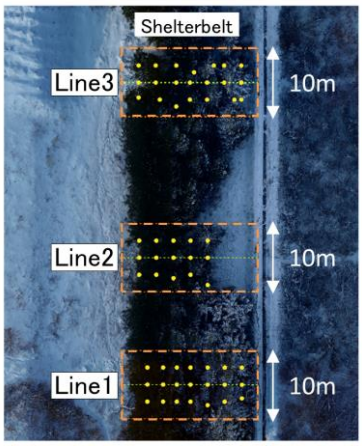

Figure 4: Ranges of belt transect (orange), and LAI measurement positions (yellow).

2.3 *Snowdrift observation*

LiDAR measurements were also conducted in mid-winter of 2022/23 on Jan. 27th, 2023 to determine the blowdown geometry of the study site, similar to the method as shown in 2.2. In addition, snowdrift surveys were conducted at the three survey lines during the snow season using snow probes with measurement scales (see Figure 1).

2.4 *Meteorological observation*

Meteorological observations were conducted during the 2022/23 winter. Measurement elements were these three; the mass flux of blowing snow using snow particle counters (SPC-95), wind velocity and direction using propeller-vane anemometers (KDC-S04), and visibility in blowing snow using transmissometers (PWD12). Each sensor was set at 1 windward side point and 3 leeward side points of the shelterbelt at a height of 1.8 m. Measurement intervals were 1 minute (wind velocity and direction, and visibility) and 1 second (mass flux of blowing snow). These data were organized as 10-minute statistics. In addition, Snow depth was measured every 10 minutes at the windward side point using a laser snow depth sensor (KDC-S18-L-10R) to grasp the distance between 1.8 m height of the each sensor and snow surface (see Figure 1). In addition, air temperature was measured using a platinum resistance thermometer, and snowfall intensity (mm h^{-1}) was measured using a Double Fence Intercomparison Reference (DFIR: Goodison et al., 1998) in the test field. These data were organized as 10-minute statistics.

3. OBSERVATION RESULTS

3.1 *Tree observation*

First, we indicated the result of LiDAR measurements (e.g., Figure 5). It was not possible to obtain the structure of the interior of the shelterbelt under each measurement condition due to the high density of leaves and branches at the observation site. In this study, the internal structure of the shelterbelt (leaves, branches, trunks, etc.) could be determined by combining the measurement profiles taken under the conditions of vertical downward (0°), oblique (45°), and lateral (60°). As an example, a cross-section of point cloud data on survey line No.1 is shown in Figure 6.

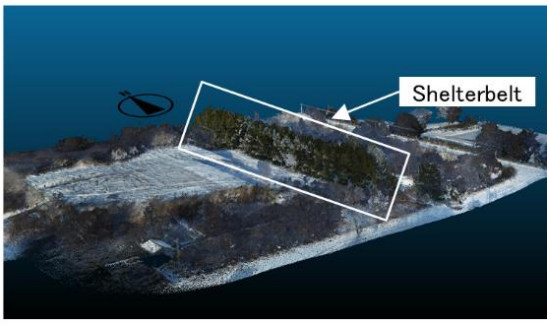

Figure 5: Aerial view of the study site looking southwest using point cloud data and camera data on Dec. 2nd, 2022.

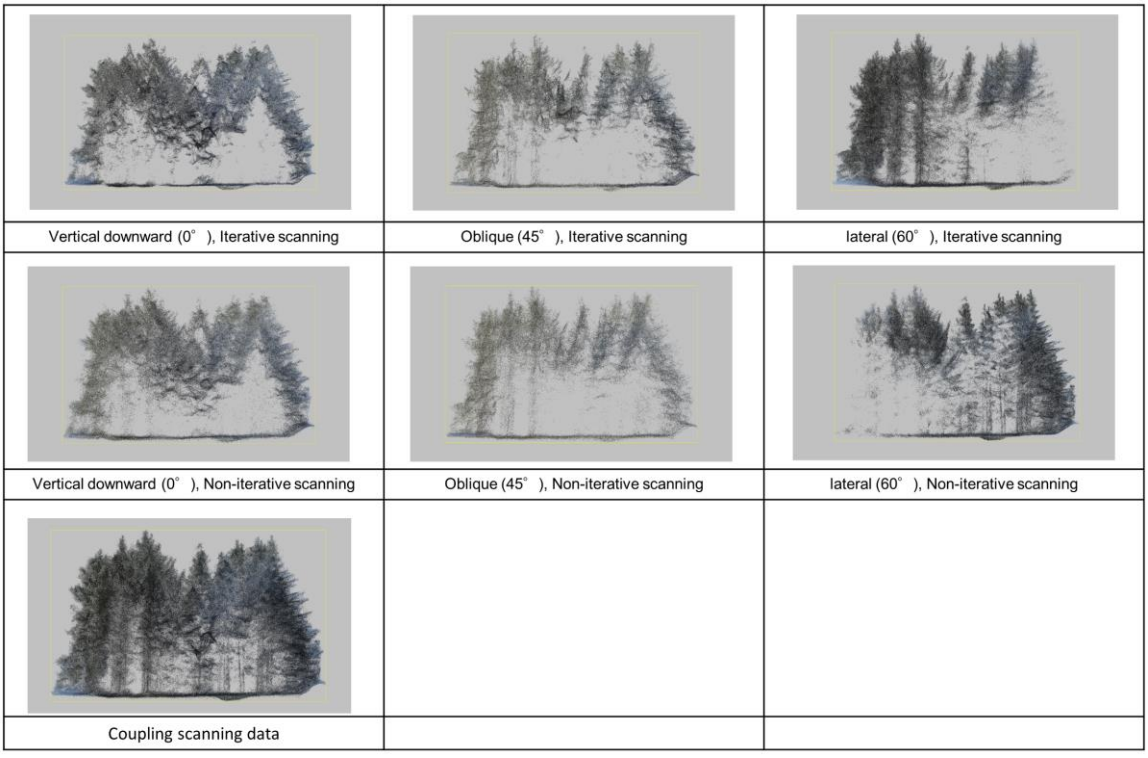

Figure 6: Cross section of point cloud data on the survey line No.1

Next, Table 1 shows the results of tree surveys and the LAI measured data by several methods for three survey lines. The characteristics of each survey line based on Table 1 are shown below.

No.1: The number of trees is the largest and the average height of the crown base (the height of the withered lower branches) is the highest in the three survey lines. The shelterbelt width and LAD are similar to No.3 and larger than No.2.

No.2: The shelterbelt width and LAD are the smallest of the three survey lines. The number of trees is similar to No.3. The average height of the withered lower branches is in between No.1 and No.3.

No.3: The average height of the withered lower branches is the smallest of the three survey lines.

3.2 Snowdrift observation

We obtained the data of the snowdrifts around the shelterbelt based on the different measurement profiles between before winter and mid-winter (Figure 7).

3.3 Meteorological observation

First, about the meteorological observation data of the windward side of the shelterbelt, the wind direction was classified as orthogonal (±67.5 to 90°), oblique (±22.5 to ±67.5°), and parallel (0 to ±22.5°) to the shelterbelt. From the orthogonal data, the data of wind speeds of 5 m s^{-1} and visibility of less than 100 m were extracted. Next, to understand the effect of the shelterbelt in a snowstorm, we selected data from three points on the downwind side at the same time as the extracted data. Using the selected data and the extracted data, the ratio of meteorological elements was organized, which were on the leeward side of the survey line No.1-3 to the windward side of the shelterbelt (see Figure 1).

Figure 8 shows box-and-whisker plots of wind speed and logarithm visibility ratios (Takechi et al., 2009) for three survey lines in the orthogonal wind direction during the observation period, with the upper and lower limits set at 1.5 times the interquartile range. The wind speed ratios were all less than 1.0, and this indicates that the wind speed was lower on the leeward side of the shelterbelt than on the windward side. The smallest wind speed ratio was No.3, followed by No.1 and No.2. In addition, a one-way analysis of variance

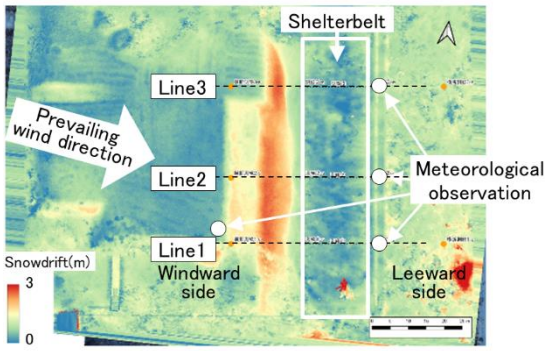

Figure 7: Snowdrift heights around the shelterbelt in mid-winter on Jan. 27th, 2023.

Table 1: Results of tree survey based on the belt transect method and several LAI measurements for survey lines No. 1-3 (TH, tree heights; BH, diameter at breast height; CW, crown width; HCB, height of crown base)

Survey Line No.	Width of the shelterbelt	Number of trees	Ave. TH	Ave. DBH	Mdn. LAI			Ave. CW	Ave. HCB
					PCA	LIA32	GLA		
1	19m	34	9.8m	14.3cm	2.95	1.50	1.75	1.67m	4.02m
2	11m	15	10.4m	15.9cm	2.30	1.35	1.68	1.87m	3.37m
3	19m	16	10.8m	18.9cm	2.91	1.77	2.84	2.18m	3.52m

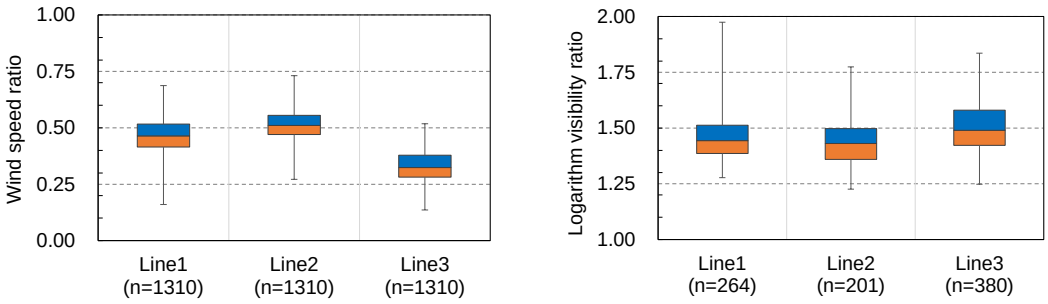

Figure 8: The ratio of meteorological elements on the leeward side on the survey line No.1-3 to the windward side of the shelterbelt, using the orthogonal wind direction, wind speeds of 5 m s^{-1} and visibility of less than 100 m data during the observation period from Dec.10th, 2022 to Mar. 10th, 2023: left, wind speed; right, logarithm of visibility.

revealed significant differences among the lines ($P < 0.01$). Next, The 25% tile value of the logarithm visibility ratio exceeded 1.35 for all lines, and the median value was the highest in No.3. This indicates that the shelterbelt reduces blowing snow from the windward side, resulting in greater visibility on the leeward side. A one-way analysis of variance revealed significant differences among the lines ($P < 0.01$).

4. ANALYSIS

4.1 Setting leaf area density using point cloud data obtained by a drone with LiDAR

The Voxel-based Canopy Profiling method (hereinafter: "VCP method") has been used to calculate leaf area density ($m^2\ m^{-3}$) (hereinafter: "LAD") from point cloud data obtained by a ground-based LiDAR (Hosoi and Omasa, 2006, 2014). In the VCP method, it estimates the LAD using the number of voxels containing the laser beam trajectory, the number of voxels containing the point where the laser beam is reflected, distribution of the leaf inclination angle. At the time, voxels that the laser beam has not passed through are excluded to improve the estimation accuracy.

The point cloud data for the shelterbelt in this study were measured from several angles by a drone moving in the sky, combined to create the data (see Figure 1 and Figure 6). In this case, the VCP method could not be applied because the trajectory of the laser beam was unknown, and the distribution of leaf inclination angle in conifer-dominated shelterbelt could not be measured. We considered that there were few areas where the laser beam did not pass through in the shelterbelt from coupled the scanning data (see Figure 6). Therefore, we set LAD using point cloud data by a drone LiDAR without using the laser beam trajectory in this study. The flow of setting is shown in Figure 9, referring to the VCP method. In this study, leaf area density ($m^2\ m^{-3}$) (hereinafter: "LAD") was calculated by dividing LAI by the average tree height (see Figure 3 and Table 1).

In Figure 9, (i) the Coordinate transformation of point cloud data at 10 m width centered on the survey line No.1 is shown in Figure 10. (ii) The space containing the shelterbelt (e.g., in the yellow frame in Figure 10) was divided into voxels, and the number of voxels containing point clouds (hereinafter: "tree voxels") was calculated for each 1-meter cubic grid (m^{-3}) so that the internal structure of the shelterbelt could be represented. (iii) Oshio et al., (2013) reported that the LAD estimated by the VCP method depends on voxel size. In this study, the number of tree voxels was organized by seven different voxel sizes: 1, 5, 10, 20, 50, 100, and 200 mm. Appropriate voxel size was investigated using the relationship between the different voxel sizes and the number of tree

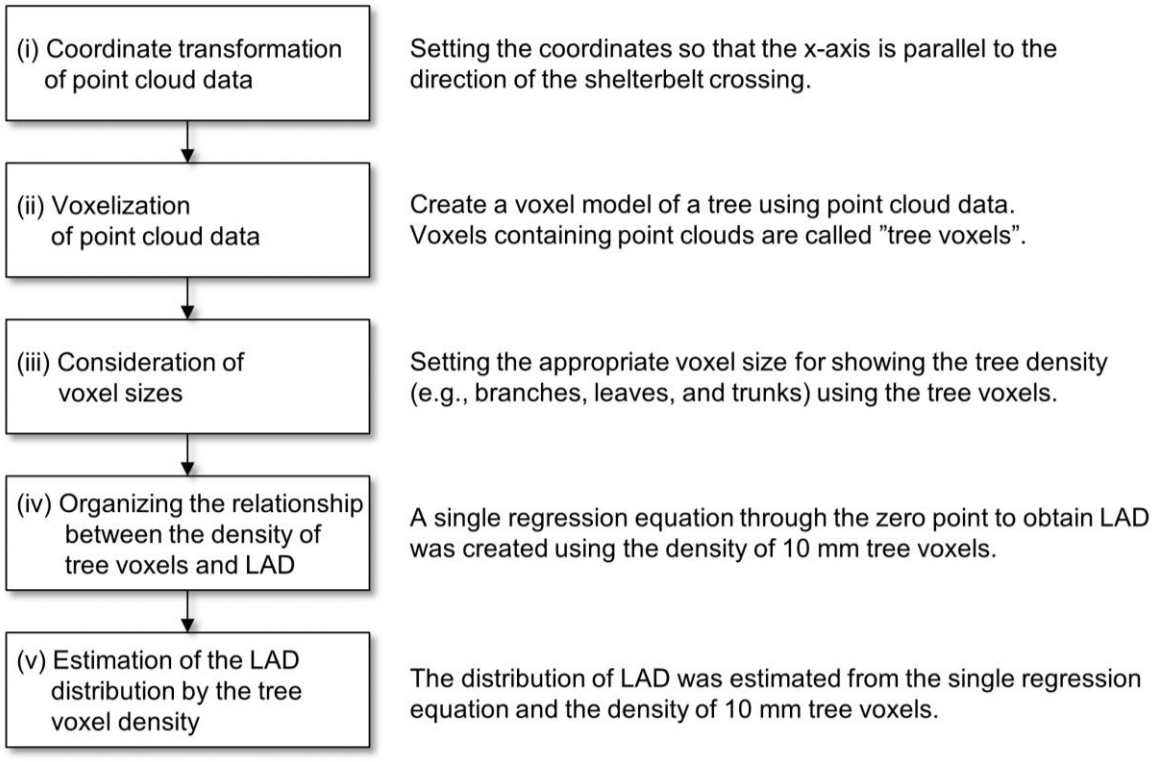

Figure 9: The flow of the setting LAD using point cloud data in this study.

voxels in a 1 m grid near the center of the shelterbelt and a grid of the edge near the ground surface. The results showed that 10 mm was the most suitable voxel size (Figure 11).

Figure 9 shows (iv) the relationship between the average density of tree voxels of 10 mm (number m^{-3}) at a 5 m radius from LAI measurement point and LAD calculated from PCA, LIA32, and GLA in the shelterbelt Interior (remove 5 m from the shelterbelt edge) is shown in Figure 12. The result shows the correlation coefficient of LAD calculated from LIA32 and calculated from GLA were about 0.6, which was statistically significant ($P < 0.01$). In this study, using the above statistically significant data, a single regression equation through the zero point was obtained.

$$LAD = 0.00014 * Dtv_{10} \quad (1)$$

Dtv_{10} is the density of 10 mm tree voxels in a 1 m cubic grid (number m^{-3}).

(v) The distribution of LAD was estimated from the equation (1) and Dtv_{10}. As an example, the Crossing direction of the average distribution of LAD on the survey line No.1 (width = 10 m, see Figure 10) is shown in Figure 13. The height from 0 m to 1 m was excluded due to the influence of the ground surface.

4.2 *Relationship between the shelterbelt and the meteorological data in a snowstorm*

To understand the relationship between the shelterbelt and meteorological data in a snowstorm, we show Table 2. It shows the correlation coefficients obtained relationship between the median value of the ratio of wind speed and logarithm visibility for lines 1-3 in the orthogonal wind direction (see Figure 8), and items of the shelterbelt based on the tree observation in Section 3.1 and the analysis results in Section 4.1.

The results show that Ave. LAD all (m^2 m^{-3}), W (m), Ave. TH (m), WTH (m^2), and WTH_LAD (m^4 m^{-3}) have a negative correlation of about 0.7 or more with the wind speed ratio and a positive correlation of about 0.7 or more with the logarithm visibility ratio. These indicate that wind speed was reduced and visibility was greater on the leeward side by the shelterbelt. In addition, the correlation coefficient of WTH_LAD was greater than WTH. This indicates the LAD contributed to the reduction of a snowstorm.

The height of the crown base (the height of the withered lower branches) shows a positive correlation of about 0.6 for the wind speed ratio and a positive correlation of about 0.6 for the logarithm

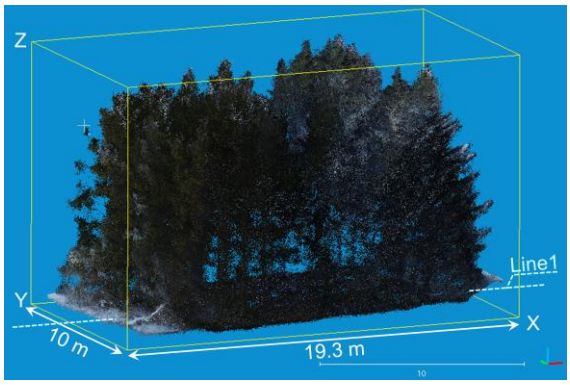

Figure 10: Coordinate transformation of point cloud data at 10 m width centered on the survey line No.1.

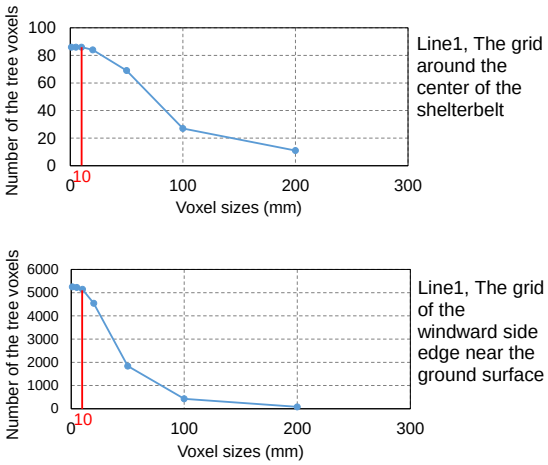

Figure 11: Relationship between the different voxel sizes and the number of tree voxels at the two different grids.

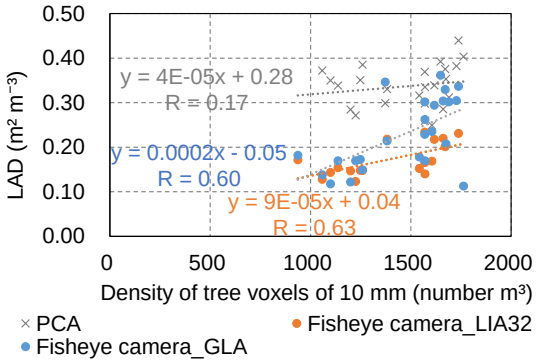

Figure 12: Relationship between the Density of tree voxels of 10 mm and the LAD calculated from PCA, LIA32, and GLA.

visibility ratio. It indicates that the wind speed was higher and the visibility was lower when the height of the crown base was higher.

On the other hand, no correlation was found for the height of 1.8 m LAD. This can be attributed that the height and width of the shelterbelt were not taken into account in this item.

Unit：m^2 m^{-3}

Survey Line1		Crossing direction from windward side to leeward side (m)																					
		0	1	2	3	4	5	6	7	8	9	10	11	12	13	14	15	16	17	18	19	20	21
TH: Tree Height (m)	16																						
	15																						
	14																						
	13																						
	12																						
	11				0.07	0.23	0.29	0.45	0.34	0.34	0.06	0.00	0.18	0.01	0.03	0.20	0.30	0.90	0.43	0.01			
	10			0.00	0.36	0.48	0.43	0.61	0.34	0.33	0.22	0.08	0.15	0.05	0.19	0.36	0.21	0.73	0.79	0.12	0.00		
	9			0.06	0.48	0.52	0.40	0.36	0.35	0.29	0.34	0.17	0.15	0.11	0.25	0.26	0.24	0.41	0.69	0.38	0.03		
	8			0.01	0.47	0.42	0.23	0.17	0.25	0.19	0.30	0.20	0.19	0.13	0.27	0.17	0.23	0.18	0.53	0.60	0.12	0.00	
	7		0.00	0.07	0.44	0.31	0.12	0.10	0.09	0.13	0.18	0.31	0.18	0.14	0.22	0.11	0.11	0.09	0.25	0.55	0.23	0.00	
	6			0.07	0.42	0.24	0.13	0.07	0.08	0.09	0.08	0.13	0.10	0.12	0.12	0.11	0.04	0.04	0.11	0.41	0.56	0.12	
	5		0.00	0.13	0.36	0.14	0.08	0.05	0.06	0.07	0.08	0.05	0.06	0.08	0.02	0.02	0.02	0.02	0.04	0.16	0.44	0.13	0.00
	4		0.03	0.27	0.32	0.12	0.08	0.04	0.04	0.03	0.02	0.03	0.06	0.03	0.02	0.01	0.01	0.04	0.04	0.08	0.35	0.29	0.00
	3		0.04	0.28	0.27	0.12	0.05	0.02	0.04	0.03	0.01	0.01	0.04	0.04	0.01	0.01	0.02	0.03	0.02	0.06	0.27	0.11	0.00
	2		0.08	0.18	0.15	0.02	0.04	0.02	0.03	0.01	0.01	0.01	0.03	0.01	0.00	0.01	0.01	0.03	0.01	0.04	0.19	0.57	0.04
	1		0.63	0.49	0.24	0.17	0.25	0.21	0.24	0.17	0.18	0.19	0.17	0.20	0.21	0.19	0.18	0.16	0.15	0.17	0.11	0.00	
	0																						

Figure 13: Crossing direction of the distribution of average LAD at 10 m width centered on the survey line No.1 (see Figure 10)

Table 2: The correlation coefficient relationship between the median value of the ratio of wind speed and logarithm visibility and items of the shelterbelt.

Items of the shelterbelt		Metrological data	
		Mdn. The ratio of	
Items	Description in the survey line No.1-No.3	Wind speed	logarithm of visibility
Ave. LAD all (m^2 m^{-3})	Average of the distribution of LAD	-0.96	0.97
Ave. LAD 1.8(m^2 m^{-3})	Average of the distribution of LAD in the height of 1 m to 3 m	-0.17	0.19
W (m)	Width of the shelterbelt	-0.69	0.68
Ave. TH (m)	Average tree heights	-0.70	0.71
Ave. BCH (m)	Average height of crown base (Average of the height of the withered lower branches)	0.58	-0.60
WTH (m^2)	Area of the survey lines W * Ave.TH (m^2)	-0.82	0.81
WTH_LAD (m^4 m^{-3})	Total leaf area of the survey lines W * Ave.TH *Ave. LAD all (m^4 m^{-3})	-0.88	0.87

5. SUMMARY AND FUTURE ISSUES

In this study, we conducted observations on trees, snowdrifts, and meteorological elements related blowing snow using a shelterbelt composed of evergreen conifers to investigate the design methodology of living snow fences in a severe snowstorm. Tree, snowdrift, and meteorological observation were conducted on three survey lines orthogonal to a linear shelterbelt in a windy and snowy area of the northern part of Japan. Based on the results, we created the average distribution of leaf area density on the survey lines and organized the relationship between the shelterbelt and the meteorological data in a snowstorm.

Going forward, we will continue the field observation in the 2023/24 winter, and analyze the field observation data for the 2022/23 and 2023/24 winters to create benchmark data for using numerical simulation of blowing and drifting snow. Based on the benchmark data, the optimal calculation conditions (boundary conditions, models, etc.) for snowstorm simulations will be discussed. We will also conduct numerical simulation of blowing and drifting snow to present an optimized configuration of living snow fences that can meet any required performance during severe snowstorm events.

REFERENCES

Civil Engineering Research Institute for Cold Region (CERI): The highway snowstorm countermeasure manual (Revised Edition 2011). Published by CERI, Public Works Research Institute, Incorporated Administrative Agency, 2011.

Oshio, H., Asawa, T., Hoyano, A. and Miyasaka, S.: Accuracy of the information on the external crown form of individual trees extracted by airborne LiDAR in urban spaces, J. Jpn. Soc. Remote Sensing, 33, 350-359, https://doi.org/10.11440/rssj.33.350, 2013. [In Japanese with English abstract]

Goodison, B.E., Louie, P.Y.T. and Yang, D.: WMO Solid Precipitation Measurement Intercomparison Final Report, WMO, WMO/TD-No.872, Instruments and Observing Methods Report No.67, 212 pp, 1998.

Hosoi, F. and Omasa, K.: (2006) Voxel-based 3-D modeling of individual trees for estimating leaf area density using high-resolution portable scanning LiDAR. IEEE Transactions on Geoscience and Remote Sensing, 44, 3610–3618, https://doi.org/10.1109/TGRS.2006.881743, 2006.

Hosoi, F. and Omasa, K.: 3-D remote sensing for measurement and analysis of forest structure, J. Jpn. Ecology, 64, 223-231, https://doi.org/10.18960/seitai.64.3_223, 2014. [In Japanese with English abstract]

Sakurai, T., Matsushima, T., Harada, Y. and Nishimura A.: Windspeed reduction at a living snow fence along a national highway estimated using optical porosity as the index, Proceedings of the XXVIIth World Road Congress (PIARC), IP0123, 1-11, 2023 [in press].

Simon Fraser University, Cary Institute of Ecosystem Studies: Gap Light Analyzer (GLA), https://www.caryinstitute.org/science/our-scientists/dr-charles-d-canham/gap-light-analyzer-gla, 1999.

Takechi, H., Matsuzawa, M. and Nakamura, H.: Relationship between human perceptions of visibility during snowstorms and values measured using transmissometers, and snow particle counters, Snow and Ice in Hokkaido, Japanese Society of Snow and Ice, Hokkaido Branch, 28, 17-20, 2009. [In Japanese]

Yamamoto, K.: LIA for Win32 (LIA32), https://www.agr.nagoya-u.ac.jp/~shinkan/LIA32/, 2005.